Case Studies in Construction Materials 4 (2016) 93–101

Contents lists available at ScienceDirect

Case Studies in Construction Materials

journal homepage: www.elsevier.com/locate/cscm

Case study

Steel scale waste as component in mortars production: An experimental study

Erika Furlani, Stefano Maschio*

Università di Udine, Dipartimento Politecnico di Ingegneria e Architettura via delle scienze 208, 33100 Udine, Italy

ARTICLE INFO

Article history:
Received 9 December 2015
Received in revised form 1 February 2016
Accepted 2 February 2016
Available online xxx

Keywords:
Steel scale waste
Recycling
Mortars
Compressive strength
Thermal conductivity

ABSTRACT

The present research reports on the results of some experiments dealing with the recycling of steel scale waste in the production of mortars. Materials were prepared mixing a commercial CEMII/B-LL cement, a steel scale waste, a commercial natural aggregate, superplasticizer and water. Natural aggregate was replaced with different proportions (5, 10, 20, 30 and 40 wt%) of steel scale waste. Water absorption, apparent density, compression strength and thermal conductivity were measured after 28 d of curing. After curing, all hydrated materials displayed: good compressive strength and low water absorption; increased apparent density with steel scale addition; improvement of thermal conductivity in materials containing up to 10 wt% steel scale addition.

1. Introduction

Industry development, population growth and the rising of consumerism have produced a rapid increase in the production of waste materials. It would be desirable to reduce waste disposal and promote recycling of waste as raw materials for other productions whenever it is possible. A large part of solid waste is produced by iron and steel industries so, if they are not properly disposed, they might damage environment and consequently have influence on human health.

Steel scale waste (SSW), a by-product of steel production, is formed on the surface of steel monoliths during their high temperature thermal treatments after casting; SSW mainly contains iron oxides and a minor fractions of other oxides as function of steel composition. This type of waste, generally known as “calamine”, is presently mainly disposed of to landfill or used to prepare counterweights concretes, due to the higher specific gravity of calamine with respect to that of all the other components that are generally used to prepare ordinary mortars or concretes.

The use of many industrial waste in concretes and/or mortars production could by-pass the problem of their landfill disposal and, at the same time, promote the production of sustainable building materials (Chowdhury et al., 2014). Alwaeli and Nadziakiewicz (2012) proposed scale and steel chips waste as a partial replacement of sand in concrete while Takeda et al. (2009) studied the physical properties of iron-oxide scales.

In the present research, mortars were produced using a fixed ratio of cement/aggregate (c/a = 1/3), as it has been often proposed in literature by other authors (Pèra et al., 1999; Qasrawi et al., 2009), whereas SSW was previously milled and transformed into a powdered product and then added in different proportions to replace part or at least all of the fine fraction of the natural aggregate.

* Corresponding author. Fax: +39 432 558251.
E-mail address: stefano.maschio@uniud.it (S. Maschio).

http://dx.doi.org/10.1016/j.cscm.2016.02.001
2214-5095/

The aim of this study is to evaluate if the addition of SSW enables to improve some properties of the hydrated mortars without paying an exaggerated cost in terms of mechanical performances or workability of the fresh pastes with respect to a reference blank composition. We also aim to demonstrate that specific gravity and thermal conductivity of the SSW containing mortars are improved with respect to the reference composition.

2. Materials and methods

The starting materials used were: a CEM II/B-LL cement, a natural aggregate with maximum particle dimension of 4.76 mm, Blaine fineness of 3480 $cm^2 g^{-1}$ (EN 933-2), density of 2.46 g cm^{-3} and water absorption 0.37% (the measurement was carried out following the ASTM C127 and C128 norms) (Maschio et al., 2011) which were mixed with different proportions of powdered SSW. The as received SSW was transformed into a powder by milling and then sieved though 1 mm, 500 μm and 200 μm sieves. The three parts of powdered steel scale were collected separately, but re-blended in such proportions as to approximate the equivalent particle size distribution of the replaced natural aggregate. In line with our previous works dealing with the production of cement based materials (Maschio et al., 2011, 2013), the Glenium 51 (BASF) superplasticizer was also used for mortars preparation. The required amount of water was added to each starting blend. The chemical analysis of cement, natural aggregate and SSW, determined by a Spectro Mass 2000 ICP mass spectrometer is reported, in terms of oxides, in Table 1 which also displays loss on ignition (LOI), obtained after thermal treatment at 1000 °C for 2 h; "undetermined" refers to the cumulative quantity of all oxides determined in quantity lower than 0.1 wt%.

The particle size distribution (PSD) of the fine fraction of the aggregate, that of CEM II/B-LL and the one of the powdered SSW was investigated by a Horiba LA950 laser scattering PSD analyzer. Analyses were made in water after a 3 min sonication and PSD curves are represented with logarithmic abscissa. In order to access the PSD of the aggregate's fine fraction, the total as received product was sieved (1000 μm) and fines were separated from coarse particles.

The crystalline phases of starting components as well as those of the hydrated materials were investigated by X-ray diffraction (XRD). XRD patterns were recorded on a Philips X'Pert Pro Detector X'celerator operating at 40 kV and 40 mA using Ni-filtered Cu-Kα radiation. Spectra were collected using a step size of 0.02° and a counting time of 40 s per angular abscissa in the range of 20–80°. Philips X'Pert High Score software was used for phase identification and semi-quantitative analysis (RIR method) (Jenkins and Snyder, 1996). In order to identify geometric shape and eventual porosity of the SSW particles, powders were examined by an Hitachi Tabletop Microscope TM3030.

The ratio between cement and aggregate quantity (natural aggregate plus SSW) was set at 1/3 in order to produce mortars with good workability and high compression strength, in line with the UNI EN 206-1, as it was previously proposed by other authors (Pèra et al., 1999; Qasrawi et al., 2009). Some reference SSW free compositions, hereafter called R, containing cement, natural aggregate, superplasticizer and an optimized amount of water were also prepared as blank samples in order to compare the mechanical behavior, after hydration, of the materials produced, bearing in mind that the focus of the present research regards the production of materials obtained by replacing part of the natural aggregate with an equivalent mass of 5, 10, 20, 30 and 40 wt% of milled and sieved SSW. Samples with symbolic names, corresponding aggregate composition, s/c and water/cement (w/c) ratios are reported in Table 2.

For the mixture preparation and w/c optimization a 5 L Hobart planetary conforming to ASTM C305 standards was used. The optimized amount of water was determined by the ASTM C1437 slump test performed on the reference blend R. The paste is said to have the right workability if the cake width is 150 (±20) mm according to UNI 7044:1972 and ASTM C230

Table 1
Chemical composition of the starting materials.

Component	Cement (wt%)	Aggregate (wt%)	SSW (wt%)
SiO_2	18.11	1.98	–
Al_2O_3	4.25	1.72	0.15
CaO	61.24	46.73	–
MgO	2.53	19.83	–
Na_2O	0.23	1.43	–
K_2O	1.10	0.74	–
FeO	–	–	96.31[b]
Fe_2O_3	3.19	2.1	–
TiO_2	0.34	–	0.47
MnO	0.56	–	1.55
Cr_2O_3	–	–	0.95
CuO	0.12	–	–
$SO^{4=}$	2.88	–	–
Cl^-	0.71	–	–
C (organic)	2.08	0.57	–
Undetermined	2.49	1.92	0.57
LOI (%)	8.24	23.55	[a]
Density (g cm^{-3})	3.08	2.46	5.65

[a] As a consequence of the thermal treatment at 1000 °C, FeO and Fe_3O_4 oxidize to Fe_2O_3.
[b] Iron is reported as FeO even if the presence of Fe_3O_4 has been detected by the XRD analysis.

Table 2
Mix proportion design.

Sample	Coarse natural aggregate (>1000 μm) (wt%)	Fine natural aggregate (<1000 μm) (wt%)	SSW 1000 μm < d < 500 μm (wt%)	SSW 500 μm < d < 200 μm (wt%)	SSW <200 μm (wt%)	s/c (%)	w/c
R	60	40	0	0	0	2	0.32
C5	60	35	2.1	1.9	1.0	2	0.32
C10	60	30	4.12	3.75	2.13	2	0.32
C20	60	20	8.25	7.5	4.25	2	0.32
C30	60	10	12.3	11.3	6.4	2	0.32
C40	60	0	16.5	15	8.5	2	0.32

norms. The identified optimal w/c value of the reference blend (R) was 0.32; this same value was applied to all the compositions. Pastes were then poured under vibration into moulds with dimensions of 100 × 100 × 100 mm, sealed with a plastic film to ensure mass curing and aged 24 h for a first hydration. Samples were then de-moulded, sealed again with a plastic film, cured again in the air for 24 h and then in water at room temperature for 28 d. The ageing water was maintained at the constant temperature of 25 °C (±3 °C) and replaced with fresh water every 3 d of curing. After curing, before their characterization, samples were dried with a cloth and aged in the atmosphere for 24 h.

Compression tests were performed after 28 d in accordance with the ASTM C39 norm using Test Mark CM8000 apparatus; data were averaged over 5 measurements. On the same samples, expansion/shrinkage was measured by a caliper.

A modified ASTM C642 norm was used to test the water absorption of the mortar samples. After ageing for 28 d, samples were put in an oven at 100 ± 5 °C for 48 h and weighed (W_1). Samples were then aged in an autoclave, at 120 °C and 2 kPa for 1 h using 2 L of water. After boiling, samples were cooled down, in water, to room temperature, dried with a cloth and weighed again (W_2). Water absorption was evaluated as: $W(\%) = 100(W_2 - W_1)/W_1$. Apparent density of the materials was determined by the Archimede's method of three 40 × 40 × 40 mm^3 specimens of each composition which were previously sealed by dropping them into a liquid paraffin bath. Averaged data have been reported.

Thermal conductivity was measured after 28 d using Hot Disk TPS 2500S instrument, with kapton 7577 sensor of 2.001 mm radius.

3. Results and discussion

The starting materials have different particle size distribution: cement displays a maximum concentration of particles at 20 μm (see Fig. 1), but contains also a little fraction of smaller particles highlighted by a small peak at around 1.5 μm; milled and sieved SSW has a PSD with a very large double peak at around 100 μm, coupled with a smaller one at around 15 μm; the natural aggregate also displays a bimodal distribution of particles with two peaks: a lower one at 10 μm and the other at around 400 μm. The PSD analysis shows that all of the starting materials contain particles of size inferior to 1000 μm and the samples prepared in the present work can be classified as mortars.

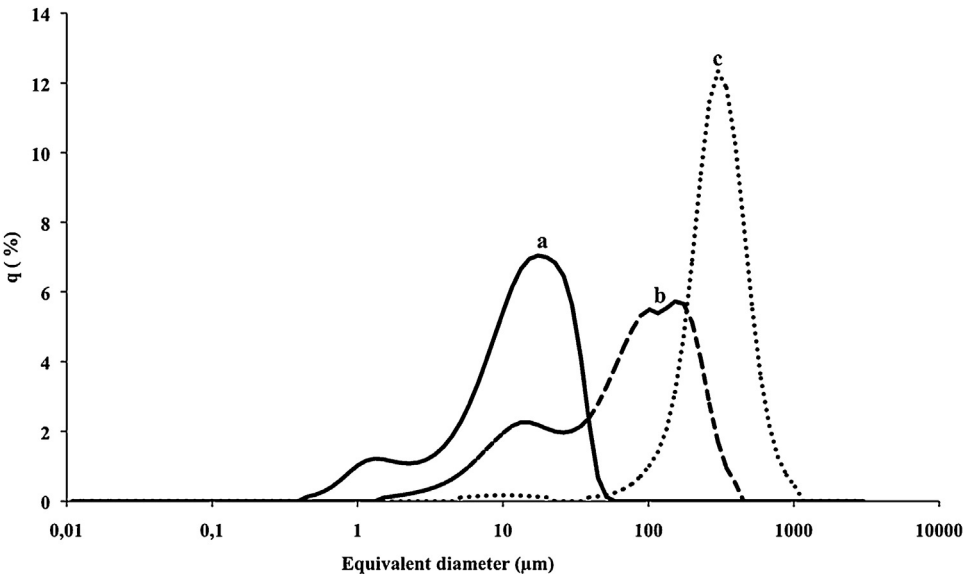

Fig. 1. PSD curves of the powdered materials used: (a) CEMII/B-LL 32.5; (b) milled and sieved SSW; (c) fine fraction of aggregate.

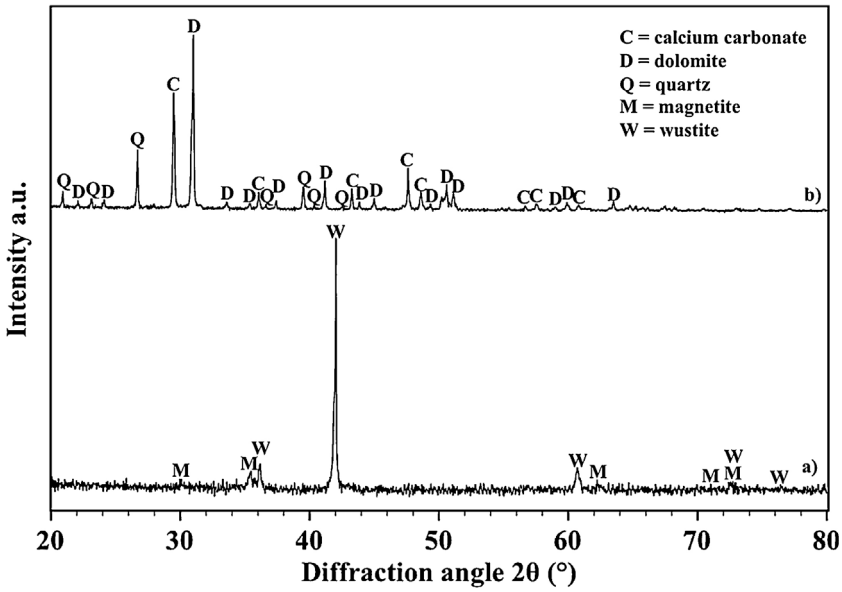

Fig. 2. X-ray diffraction patterns of steel scale waste (a) and aggregate (b).

SSW mainly contains iron oxide (97.88%) and very low amount of other oxides (e.g. MnO, TiO_2 and Cr_2O_3). Aggregate mainly contains calcium oxide, magnesium oxide with small fractions of free silica, alumina and sodium oxide. Organic carbon, density and LOI of cement and aggregate are in line with literature data (Neville and Brooks, 1990; Collepardi, 1991); CEM II/B-LL conforms to European Standards EN-197/1. Data reported in Table 1 are confirmed by the XRD analysis which revealed the presence of alite (84%) and belite (16%) in cement, dolomite (65%), calcium carbonate (27%) and free quartz (8%) in the aggregate whereas wustite (92%) and magnetite (8%) were identified in SSW (Fig. 2); however the above numbers only supply an approximate crystallographic composition because XRD does not provide accurate quantitative analysis.

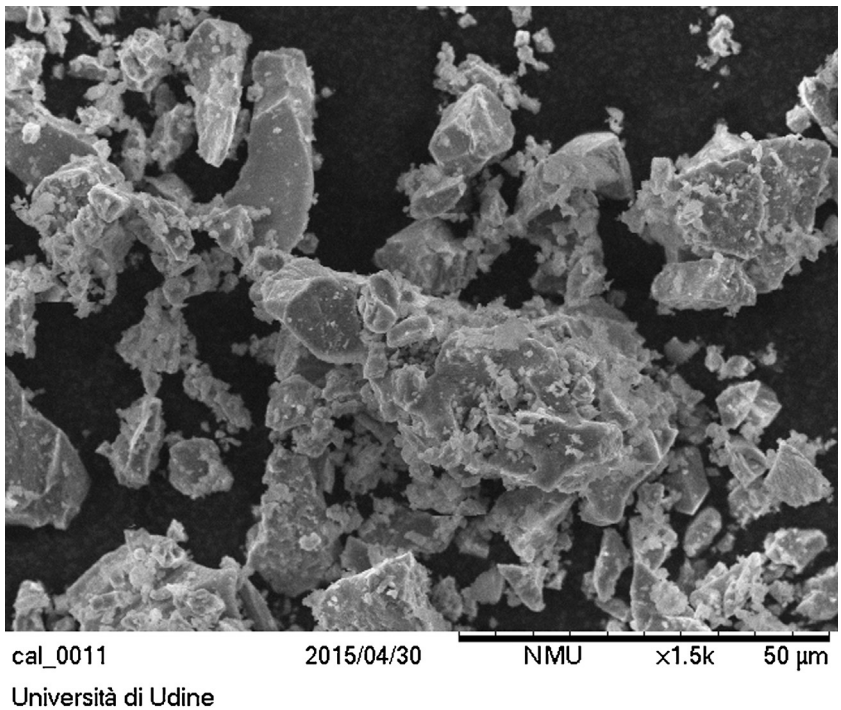

Fig. 3. SEM micrograph of milled and sieved SSW.

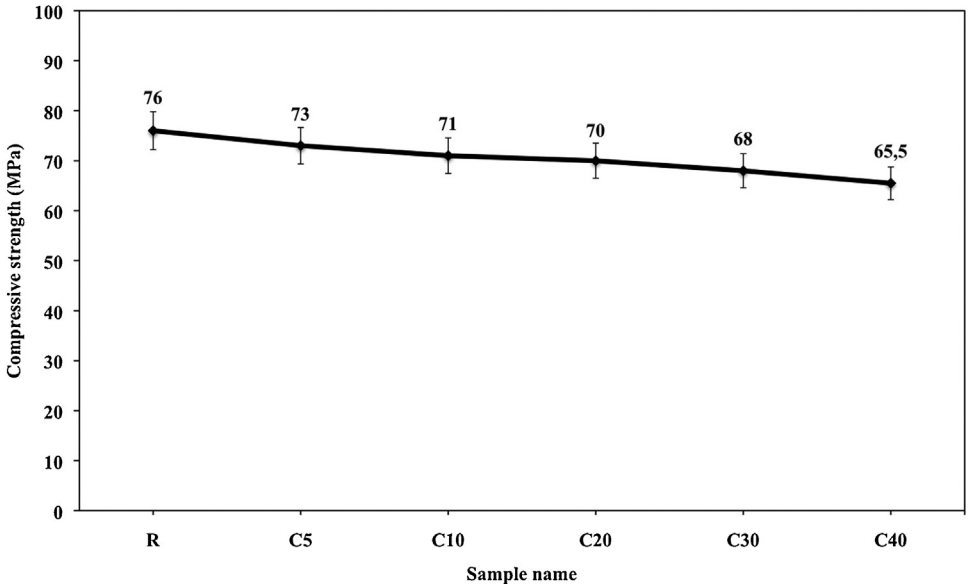

Fig. 4. Compressive strength as a function of SSW addition of the samples after 28 d of curing.

Fig. 3 is a SEM micrograph of the finest fraction of SSW, the one with particle size inferior to 200 μm. It is possible to observe soft clusters of particles ranging from 1 to more than 50 μm, but each single particle appears pore-free and of irregular shape. It follows that the addition of calamine little affects w/c ratio during materials production.

In order to limit the number of variables during materials preparation, as it has been reported in the experimental section, the as received SSW was transformed into a powder by milling and then sieved though 1 mm, 500 μm and 200 μm sieves. The three parts of powdered steel scale were collected separately, but re-blended in such proportions as to replicate the equivalent particle size distribution of the replaced natural aggregate.

Due to the different density of natural aggregate and calamine, blends containing SSW had similar, but not same rheological behavior as the reference composition. In fact SSW tends to segregate when pastes are worked and then poured into the mould. Segregation results much more evident in samples containing the highest amount of SSW i.e. compositions C30 and C40.

Fig. 4 shows the trend of compressive strength as a function of the added amount of calamine (error bars are also reported). It can be observed that data scattering is, for each composition, maintained within the interval ± 5% of the average

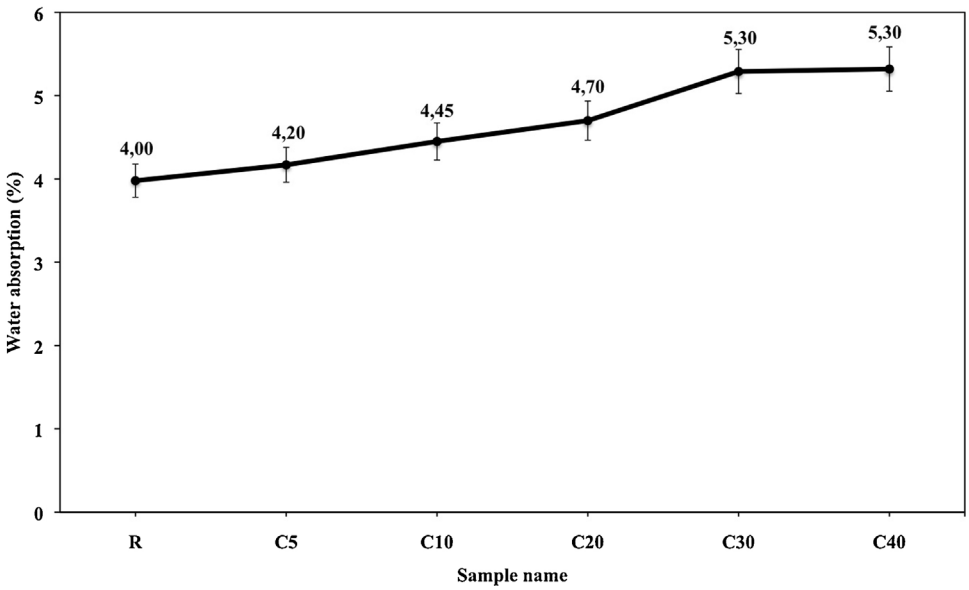

Fig. 5. Water absorption as a function of SSW addition after 28 d of curing.

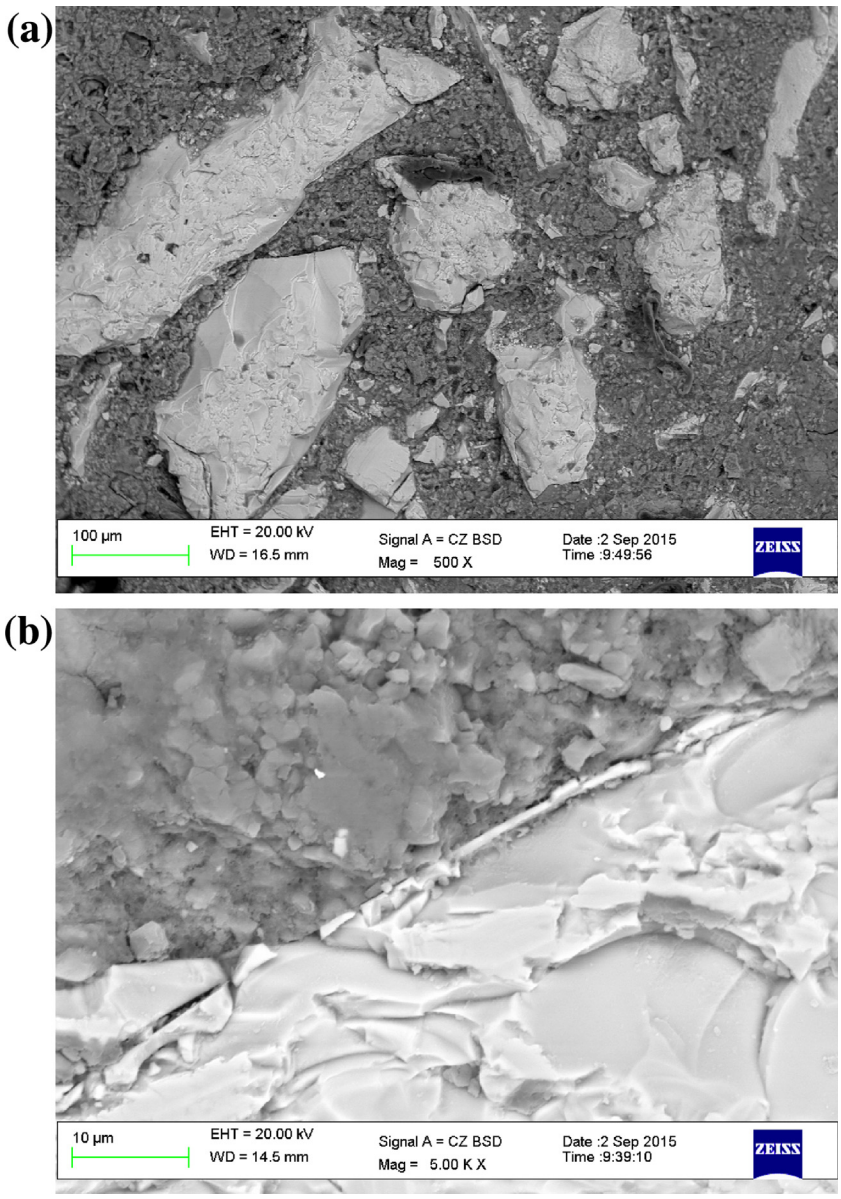

Fig. 6. (a) SEM micrograph of the fracture surface of a C10 sample; (b) detail of the interface between a calamina particle and the surrounding material.

value. It can be also remarked that, increasing the amount of calamine, the corresponding compressive strength slightly decreases and ranges from a maximum of 76 MPa of the reference sample (R) to a minimum of 65.50 MPa of sample C40. According to UNI EN 206-1 standard, compression strength values greater than 60 MPa permit to classify as high performance cement based materials, the mortars prepared in the present work. Such high compressive strength data are reasonably due to the characteristics of the natural aggregate used in the present research (Husem, 2003) and to the preparation protocol followed. It was also verified that steel scale addition did not cause shrinkage/expansion changes with respect to the reference composition.

Fig. 5 shows water absorption as a function of the of the amount of SSW added (error bars are also displayed). Water absorption increases with an almost linear trend as increasing the amount of SSW in the samples. In particular, it ranges from 3.98% of samples R to 5.32% of those with composition C40. It must be pointed out that water absorption is not porosity, but is related to the open porosity; moreover a body contains open porosity as well as closed porosity. The water absorption test provides access to the open, but not to the closed porosity which remains undetermined together with materials total porosity. However, we would like to point out the strict relationship between compressive strength and water absorption data which are relatively low in all the samples. This result is consequence of the low w/c ratio which can be achieved by the addition of the superplasticizer during mortars preparation.

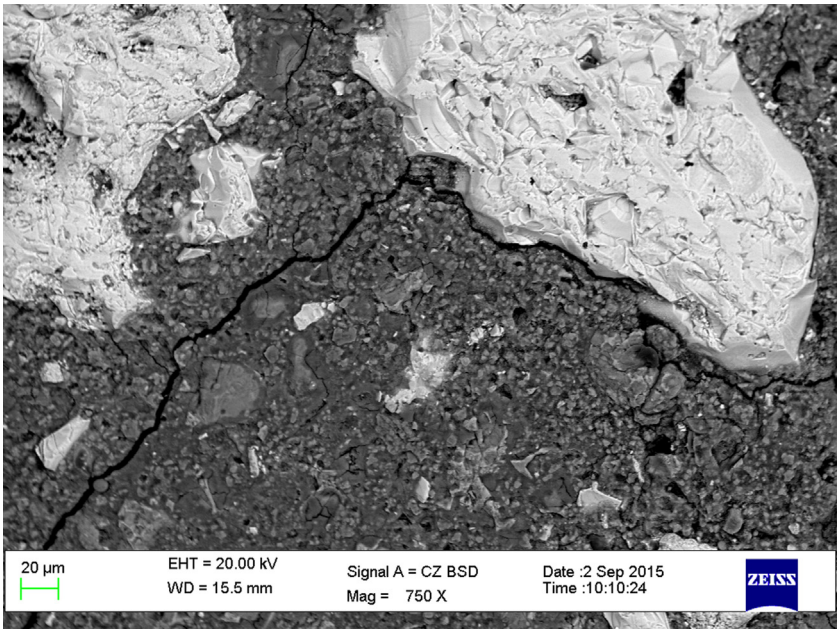

Fig. 7. SEM imagine of a crack tip deflected by a calamine particle.

Fig. 6a is a back scattered SEM image of the fracture surface of a sample with composition C10 and shows that the presence of calamine particles does not induce formation of cracks or fractures at the interface which appears well defined as it is clearly documented by Fig. 6b thus in agreement with the results obtained by other authors (Valore Rudolph, 1977; von Szadkowski, 1980). It is therefore reasonable that the greater water absorption of compositions C20, C30 and C40 with respect to R, C5 and C10 is mainly due to the greater segregation of large calamine particles during materials preparation which occurs in the former three compositions.

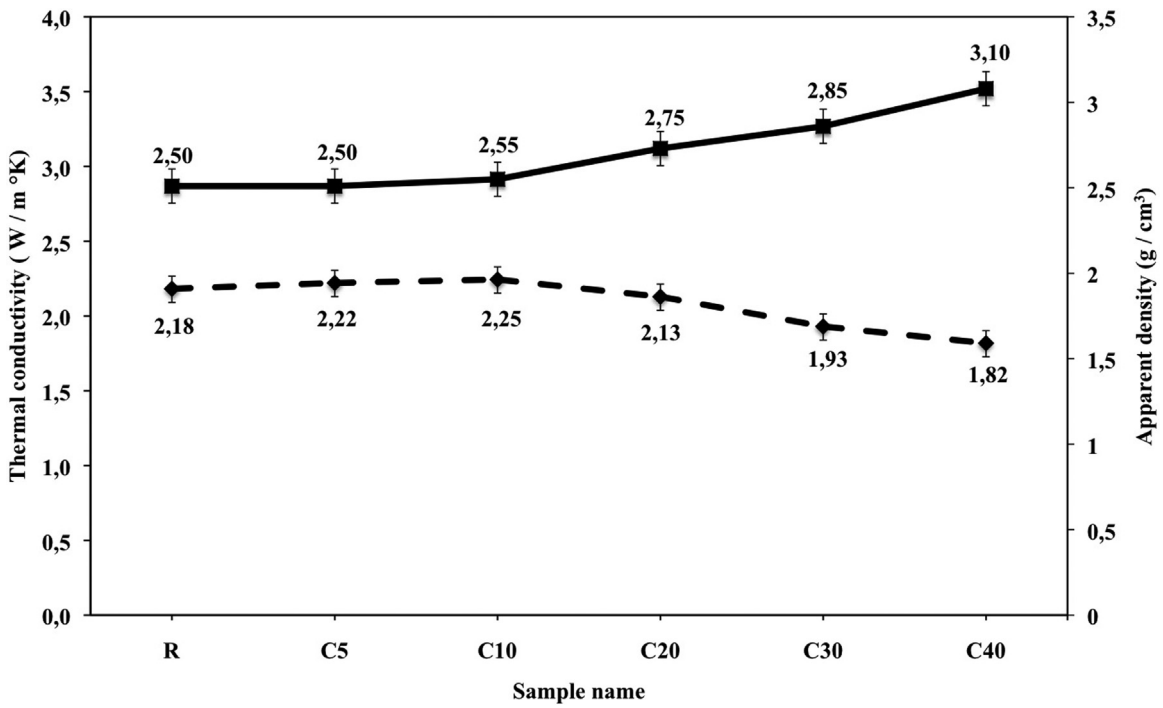

Fig. 8. Apparent density (plain line) and thermal conductivity (dashed line) as a function of SSW addition of the materials after 28 d of curing.

It has been also observed that calamine particles are able to deflect the propagating fractures from their original direction as it is documented in Fig. 7 so that it is possible to speculate, in agreement with literature (Wahi and Ilschner, 1980; Chen and Chen, 1992; Pezzotti et al., 1996; Das et al., 2015; Kumar and Barai, 2011; Nallathambi and Karihaloo, 1986), that their presence could concur to build up materials fracture toughness without compromising strength as it is demonstrated by data displayed in Fig. 4.

Fig. 8 displays apparent density as a function of SSW additions of hardened mortars specimens. As expected, due to the higher specific gravity of calamine with respect to the value of the natural aggregate, increasing amounts of SSW additions, also increases material's apparent density which ranges from 2.50 g cm^{-3} of the reference blank samples to 3.10 of materials with composition C40.

Fig. 8 also shows the trend of materials thermal conductivity vs materials composition. It is possible to see that the values increase from 2.18 W m^{-1} K^{-1} of R sample to 2.22 W m^{-1} K^{-1} of the composition containing 5% of SSW and 2.25 of C10 and than it decreases progressively to 2.13 of C20, 1.93 of C30 and 1.82 of C40 sample. Takeda et al. demonstrated (Takeda et al., 2009) that the thermal conductivity of SSW is around 5 W m^{-1} K^{-1} whereas literature reports that the one of an ordinary concrete ranges from 1.7 to 2.5 W m^{-1} K^{-1} according to International Standard EN-ISO 10456:2007. As a consequence of the addition of SSW, the improvement of thermal conductivity results therefore almost limited both as absolute and relative values.

Other authors (Vincenta et al., 2012; Wang et al., 2006; Carson et al., 2005; Lima et al., 2005; Koronthalyova and Matiasovsky, 2003) demonstrated that thermal conductivity and residual porosity are interdependent. Porosity affects thermal conductivity depending of its volumetric fraction and such effects could be classified into three ranges: the first between 0 and 6% of porosity showing linear decrease of conductivity with low slope; the second, between 6 and 9% displaying steep decrease of conductivity and the third, over 9% showing linear decrease with a slope larger than that in the first range. It is therefore generally accepted that the thermal conductivity decreases as volume fraction of porosity increases; however, in the second interval (6–8%), the decrease is generally much steeper than in the two others. Such a behavior could be explained taking into account the presence of interconnected open pores in the third interval of porosity whereas closed pores seem to influence thermal conductivity in the first range; transition occurs in the second.

As reported above, the water absorption method, which has been used in the present research to investigate open porosity, does not reveal the total porosity of materials because closed porosity remains undetermined. It follows that, in the present discussion, we can only speculate that materials with composition R, C5 and C10, which display similar low water absorption level, do not contain interconnected open porosity and belong to materials which display behavior classified into the first range of porosity, i.e. the one between 0 and 6%. As a consequence, it is reasonable to conceive that their thermal conductivity is poorly affected by porosity and more by the addition of powdered SSW. Conversely, specimens with composition C20, C30 e C40 suffer of greater porosity than R, C5 and C10 and the effects of powdered SSW additions are therefore minimized: it follows that their thermal conductivity results lower that that of the reference material.

As a conclusive remark, it is possible to state that all materials prepared in the present research do not suffer of a significant decrease of their mechanical strength as effect of the SSW additions. It appears moreover reasonable that the decrease of compression strength which has been observed in materials containing the highest amount of calamine could be mainly due to the increase of their residual porosity, more than as effect of the SSW addition. However, it cannot be neglected that calamine increases the specific gravity of the materials in which segregation was observed during mortar pastes preparation.

As reported by other authors (Valore Rudolph, 1977; Ling et al., 2012), it is important to point out that mortars with high specific gravity could be suitable for constructions related to nuclear power plants. In fact, such concretes could better attenuate neutrons and gamma rays. Such properties should concur with improved thermal conductivity, low cost, high density, ease of fabrication and good structural properties. Most of the above characteristics have been obtained in the materials prepared in present research.

4. Conclusions

In the present research the production of stable mortars was carried out using a commercial cement, steel scale waste, natural aggregate, superplasticizer and water. Mortars were produced using fixed w/c, c/a, s/c ratios whereas SSW was added in different proportions.

The following important conclusions were derived from the study:

1. All hydrated materials displayed high compressive strength after 28 d of curing as a consequence of their low water absorption so that they all could be classified as high performing mortars; however strength progressively decreases with increasing the addition of SSW;
2. Due to greater specific gravity of SSW with respect to that of the natural aggregate, materials apparent density displayed an increasing trend as a function of SSW addition;
3. Samples containing 5 and 10% of SSW showed the highest thermal conductivity values which was explained taking account of the higher thermal conductivity of SSW if compared to the one of an ordinary concrete coupled with their low water absorption (low open porosity).

Acknowledgements

Dr. Cossi Riccardo, Dr. ssa Dagmar Bilaničová and Dr. ssa Ricci Loretta of Qi srl (Pomezia—ROME) are gratefully acknowledged for thermal conductivity measurements.

Mr. Nicola Patron of Labware Tools (Treviso) is gratefully acknowledged for SEM Benchtop Hitachi demo.

References

Alwaeli, M., Nadziakiewicz, J., 2012. Recycling of scale and steel chips waste as a partial replacement of sand in concrete. Constr. Build. Mater. 28, 157–163.
Carson, K., Lovatt, S.J., Tanner, D.J., Cleland, A.C., 2005. Thermal conductivity bounds for isotropic, porous materials. Int. J. Heat Mass Trans. 48, 2150.
Chen, P.L., Chen, I.W., 1992. In-situ alumina-aluminate platelet composites. J. Am. Ceram. Soc. 75 (9), 2610–2612.
Chowdhury, S., Roy, S., Maniar, A.T., Suganya, O., 2014. Comparison of mechanical properties of mortar containing industrial byproduct. APCBEE Proced. 9, 317–322.
Collepardi, M., 1991. Scienza e Tecnologia del Calcestruzzo, 3rd ed. Hoepli ed, Milan (Italy) (in Italian).
Das, S., Kizilkanat, A., Neithalath, N., 2015. Crack propagation and strain localization in metallic particulate-reinforced cementitious mortars. Mater Design 79, 15–25.
Husem, M., 2003. The effects of bond strengths between lightweight and ordinary aggregate-mortar, aggregate-cement paste on the mechanical properties of concrete. Mater. Sci. Eng. 63, 152–158.
Jenkins, R., Snyder, R., 1996. Introduction to X-ray Powder Diffractometry. Wiley, New York.
Koronthalyova, O., Matiasovsky, P., 2003. Thermal conductivity of fibre reinforced porous calcium silicate hydrate-based composites. J. Build. Phys. 27, 71–89.
Kumar, S., Barai, S.V., 2011. Concrete Fracture Models and Applications. Springer, Verlag, Berlin Hidelberg (Germany).
Lima, W.M., Biondo, V., Weinand, W.R., Nogueira, E.S., Medina, A.N., Baesso, M.L., Bento, A.C., 2005. The effect of porosity on thermal properties: towards a threshold of particle contact in sintered stainless steel. J. Phys-Condens. Matter 17, 1239.
Ling, T.-C., Poon, C.-S., Lam, W.-S., Chan, T.-P., Fung, K.K.-L., 2012. Utilization of recycle cathode ray tubes glass in cement mortar for X-ray radiation-shielding applications. J. Hazard. Mater. 199–200, 321–327.
Maschio, S., Tonello, G., Piani, L., Furlani, E., 2011. Fly and bottom ashes from biomass combustion as cement replacing components in mortars production: rheological behaviour of the pastes and materials compression strength. Chemosphere 85, 666–671.
Maschio, S., Tonello, G., Furlani, E., 2013. Recycling glass cullet from waste CRTs for the production of high strength mortars. J. Waste Manag. 2013 (8 pages Article ID 102519).
Nallathambi, P., Karihaloo, B.L., 1986. Determination of specimen-size independent fracture toughness of plain concrete. Mag. Concr. Res. 38 (135), 67–76.
Neville, A.M., Brooks, J.J., 1990. Concrete Technology. Longman, London (UK).
Pèra, J., Husson, S., Guillot, B., 1999. Influence of finely ground limestone on cement hydration. Cement Concrete Res. 21, 99–105.
Pezzotti, G., Okamoto, Y., Nishida, T., Sakai, M., 1996. On the near-tip toughening by crack-face bridging in particulate and platelet-reinforced ceramics. Acta Metall. Mater. 44 (3), 899–914.
Qasrawi, H., Shalabi, F., Asi, I., 2009. Use of low CaO unprocessed steel slag in concrete as fine aggregate. Constr. Build. Mater. 23, 1118–1125.
Takeda, M., Onishi, T., Nakakubo, S., Fujimoto, S., 2009. Physical properties of iron-oxide scales on Si-containing steels at high temperature. Mater. Trans. 50 (9), 2242–2246.
von Szadkowski, G., 1980. The effect of pigments on the quality of concrete blocks. Proc 1st Int. Conf. on CBP, 09 155–156.
Vincenta, C., Silvaina, J.F., Heintza, J.M., Chandrab, N., 2012. Effect of porosity on the thermal conductivity of copper processed by powder metallurgy. J. Phys. Chem. Solids 73 (3), 499–504.
C. Valore Rudolph, Methods of preparing iron oxide mortars or cements with admixtures and the resulting products, US 4188231A (1977).
Wahi, R.P., Ilschner, B., 1980. Fracture behaviour of composites based on Al_2O_3-TiC. J. Mater. Sci. 15, 875–885.
Wang, J., Carson, J.K., North, M.F., Cleland, D.J., 2006. A new approach to modelling the effective thermal conductivity of heterogeneous materials. Int. J. Heat Mass. Trans. 49, 3075.